Giant optical nonlinearity of Fermi polarons in atomically thin semiconductors

Liuxin Gu[1,*], Lifu Zhang[1,*], Ruihao Ni[1], Ming Xie[2], Dominik S. Wild[3], Suji Park[4], Houk Jang[4], Takashi Taniguchi[5], Kenji Watanabe[6], Mohammad Hafezi[7], You Zhou[1,8,†]

[1]Department of Materials Science and Engineering, University of Maryland, College Park, MD 20742, USA

[2]Condensed Matter Theory Center, University of Maryland, College Park, MD 20742, USA

[3]Max Plank Institute of Quantum Optics, Garching, 85748, Germany

[4]Center for Functional Nanomaterials, Brookhaven National Laboratory, Upton, NY 11973, USA

[5]Research Center for Electronic and Optical Materials, National Institute for Materials Science, 1-1 Namiki, Tsukuba 305-0044, Japan

[6]Research Center for Materials Nanoarchitectonics, National Institute for Materials Science, 1-1 Namiki, Tsukuba 305-0044, Japan

[7]Joint Quantum Institute (JQI), University of Maryland, College Park, MD 20742, USA

[8]Maryland Quantum Materials Center, College Park, Maryland 20742, USA

*These authors contributed equally to this work.

†To whom correspondence should be addressed: youzhou@umd.edu

Realizing strong nonlinear optical responses is a long-standing goal of both fundamental and technological importance. Recently significant efforts have focused on exploring excitons in solids to achieve nonlinearities even down to few-photon levels. However, a crucial tradeoff arises as strong light-matter interactions require large oscillator strength and short radiative lifetime of excitons, which limits their nonlinearity. Here we experimentally demonstrate strong nonlinear optical responses with large oscillator strength by exploiting the coupling between excitons and carriers in an atomically thin semiconductor. By controlling the electric field and electrostatic doping of trilayer WSe_2, we observe the hybridization between intralayer and interlayer excitons and the formation of Fermi polarons. Substantial optical nonlinearity is observed under continuous wave and pulsed laser excitation, where the Fermi polaron resonance blueshifts by as much as ~10 meV. Intriguingly, we observe a remarkable asymmetry in the optical nonlinearity between electron and hole doping, which is tunable by the applied electric field. We attribute these features to the optically induced valley polarization due to the interactions between excitons and free charges. Our results establish atomically thin heterostructures as a highly versatile platform for engineering nonlinear optical response with applications to classical and quantum optoelectronics.

Nonlinear optical phenomena lie at the heart of classical and quantum optics, with applications ranging from data communications to quantum control[4,5]. Developing physical systems with stronger optical nonlinearity while reducing their power requirement holds the promise for more efficient optoelectronics and may unlock new technologies such as single-photon switches and transistors[6–8]. In recent years, significant efforts have been devoted to investigating excitons in semiconductors as a solid-state medium for realizing strong optical nonlinearity[1–3].

Van der Waals heterostructures based on atomically thin transition metal dichalcogenides (TMDs) have emerged as a new platform for fundamental studies of excitons and for engineering optical responses[9,10]. Excitons in such two-dimensional materials are highly tunable with rich spin-valley physics and possess characteristics promising for optical nonlinearity, such as strong light-matter interactions and weak screening of Coulomb potential[10]. However, a major challenge in achieving high nonlinearity under low excitation power arises from the balance between the strengths of exciton-photon and exciton-exciton interactions[11–13]. For instance, intralayer excitons in these materials exhibit large oscillator strength but experience weak interactions, dominated by exchange interactions and limited by their short lifetime[14]. On the other hand, interlayer excitons in TMD heterostructures have longer lifetimes and experience interactions due to their finite electric dipole moment[15,16]. Unfortunately, spatial separation of the electron-hole wavefunctions leads to weaker absorption of incident photons. Several recent studies demonstrated enhanced the interlayer exciton absorption via its hybridization with intralayer excitons in MoS_2[1,17–19], although the oscillator strength of such hybrid excitons is still an order of magnitude weaker than the intralayer ones. So far, strong nonlinearity in the intralayer excitons has not yet been realized. In this study, we report giant nonlinear optical responses of intralayer charged excitons, *i.e.,* Fermi polarons, on the order of several millielectronvolts under photon flux of 10^{13} photons per second

per square micrometer. The strong nonlinearity is highly tunable by doping and electric field, based on which we attribute the nonlinearity to an optically induced valley polarization resulting from exciton-carrier scattering.

Results

Electrical control of excitons

In our experiments, we encapsulate exfoliated WSe_2 homotrilayersinside two layers of hBN in a dual-gate geometry to independently control the overall doping levels and the displacement field (**Fig. 1a & b**). **Figure 1c** shows the photoluminescence (PL) map of the sample by varying the electric field while keeping the samples undoped. We observe strong emission from excitons X_I, whose energy linearly shifts with electric field from 1.58 eV to 1.50 eV, and PL peaks at 1.71, 1.55 and 1.52 eV that remains constant with varying electric field. We attribute the peak at 1.71 eV to intralayer momentum-direct exciton X_A at the K-K transition, based on their strong absorption (**Fig. 1d**) and zero Stark shift. The lower energy of X_I indicates that they are momentum-indirect excitons at the band edge, corresponding to transition across the indirect gap, located at the valence band Γ and conduction band Q valleys, according to the band structure calculations[20–22]. From the linear Stark shift, we estimate the electric dipole of X_I to be around 0.78 $nm \cdot e$ (see Methods). The corresponding vertical displacement of the electron-hole pair in X_I is approximately half of the distance between the top and bottom tungsten layers, indicating the electrons or holes are partially layer delocalized.

Next, we measure the reflectance of the trilayer under an electric field (**Fig. 1d**). In addition to the intralayer X_A, we observe an additional reflectance contrast at 1.78 eV (IX_D), which exhibits a substantial Stark effect of almost 100 meV (additional devices shown in **Fig. S1**). The finite

reflection contrast and linear Stark effect of IX_D suggest that it corresponds to interlayer exciton at the direct K-K transition with larger oscillator strength than those momentum-indirect excitons, X_I, observed in PL. From the slope of the Stark effect, we estimate the electron-hole displacement to be 1.35 nm. Interestingly, as the energy of IX_D approaches that of the intralayer exciton X_A under a higher electric field, we observe an apparent anti-crossing behavior of X_A and IX_D near the electric field of 0.05 V/nm. We note that the levels are not fully avoided and there is always finite reflection from X_A at 1.71 eV for all electric fields, which will be discussed in more depth later. To quantitatively understand the avoided crossing, we extract the exciton energies by fitting reflectance spectra and then model the anti-crossing using a simple coupled oscillator model, from which we estimate a coupling strength of $W = 10 \pm 2$ meV between X_A and IX_D (**Fig. S2**).

We further characterize how electrostatic gating modifies intralayer excitons X_A and their hybridization with interlayer excitons. **Figure 1d** shows the doping-dependent reflectance spectra of the sample under zero electric field. Upon doping, the reflectance from neutral X_A diminishes as they lose their oscillator strength, and the charged intralayer excitons emerge and shift to lower energies, with similar behaviors observed in PL (**Fig. S3**). The redshift of charged excitons with increasing doping levels can be explained in terms of attractive Fermi polaron[23], or an increase in the exciton-trion energy splitting with increasing Fermi energy[24]. The similar doping dependence of reflectance and PL is due to the absence of Pauli blocking in both cases when the free carriers do not reside in the K valley[25]. As we focus on the highly doped regime where excitons interact with a large number of carriers, we refer to these charged excitons as Fermi polarons in later discussions[23].

Giant optical nonlinearity

Next, we study the excitons' nonlinear optical response by measuring the sample's reflectance spectra under different laser pumping. **Figures 2a-c** show the reflectance spectra of the sample, probed with a halogen lamp, while we excite the system with a 635nm continuous wave (CW) laser of different power. When the trilayers are electron-doped or intrinsic, optical pumping does not alter the reflectance spectra significantly. Intriguingly, however, in the hole-doped regime, optical pumping leads to a dramatic blueshift of the Fermi polaron X_A^+, on the order of a few millielectronvolts, and a slight linewidth increase under tens of microwatts excitation (**Fig. 2b**). The oscillator strength of X_A^+, extracted from the reflection spectra, remains almost constant at low excitation power and decreases at higher power (**Fig. S4**). We note that PL signals are more than four orders of magnitude weaker than the reflected light and therefore negligible.

To visualize the doping dependence of nonlinearity, we measure the relative change in the sample's reflectance induced by the optical pumping, $\Delta R/R = R_p/R_{np} - 1$, where R_p and R_{np} are the sample's reflectance spectra with and without the laser pumping, respectively. **Figure 2d** shows the reflectance spectra $\Delta R/R$ under symmetric gating with zero electric field, where we observe a striking asymmetry between the electron and hole sides. We briefly note that our observed nonlinearity of intralayer excitons is orders of magnitude stronger than that of dipolar interlayer excitons in bilayer TMDs[19,26] (see Table S1 for detailed comparison with other systems). Another critical distinction is that the nonlinearity in bilayer TMDs occurs for interlayer excitons in the intrinsic regime[1,19].

In addition to non-resonant excitation, we also probe the optical nonlinearity by resonantly exciting X_A with a pulsed laser (718 to 730 nm wavelength, ~100 ps pulse duration) and observe qualitatively similar nonlinear behaviors with a ~10 meV blueshift of X_A^+ and an increase in its

linewidth, only on hole-doped side (**Figs. 2e & S5**). To investigate how excitation photon energies impact the nonlinearity, we tune the pulsed laser energy across the X_A^+ resonance. Resonant excitation results in a stronger blueshift than higher energy excitation, while there is no noticeable shift in X_A^+ when the photon energy falls below X_A^+ (**Fig. S6**). Additionally, we observe no significant wavelength dependence when the photon energy exceeds X_A^+ (**Fig. S6**). Notably, the pulsed excitation generates an order of magnitude smaller blueshift than the CW laser at lower power with its peak power comparable to the CW laser's average power (**Fig. S8**).

Optically induced valley polarization

The observed Stark effect and anti-crossing in WSe_2 trilayers can be understood by examining their crystal and band structure. In trilayers, each monolayer is rotated 180 degrees, resulting in alternating K and K' points between layers[27] (**Figs. 3a, b**). Here we mainly consider the hole tunnelling process, which is predicted to be much stronger than electron tunnelling by density functional calculations[28]. The sizeable spin-orbit coupling in the valence band dictates that the direct tunneling between the neighboring layers would be much weaker than that between the top and bottom layers across the middle layer (**Fig. 3a, b**). Such tunneling leads to finite oscillator strength of interlayer K-K excitons IX_D and their avoided crossing with intralayer X_A[29]. Indeed, the experimentally extract coupling strength between X_A and IX_D is consistent with the calculated interlayer coupling strength of holes at the K valley[22]. This picture is further corroborated by our measured dipole moment of IX_D being close to the distance between the top and bottom layers, and explains our observation that the level crossing at X_A is not fully avoided, since IX_D does not couple to intralayer excitons in the middle layer.

The observed optical nonlinearity and their doping dependence cannot be simply explained by heating or carrier injection from the laser since both effects result in redshift of the intralayer excitons (**Figs. 1e & S9**). Therefore, we examine how the interactions among the elementary excitations in the systems, *i.e.,* intralayer excitons X_A, momentum-indirect excitons X_I, and free carriers, may give rise to the observed nonlinearity. First, we extract a large interaction strength g ~ 2 meVμm^2 from the linear fit of energy blueshift vs. X_A^+ density at low power[30] (**Fig. S8**). It is apparent that excitonic interactions (*i.e.* between X_A-X_A and X_A-X_I) alone cannot produce the observed nonlinearity. On the one hand, the X_A-X_A interactions among intralayer excitons are repulsive but weak, which scales linearly with density with a coefficient of g_{ex}~ $\alpha E_B R^2$~1.9μeVμm^2, where α is a constant (~6), $E_B \approx 100$ meV is the exciton binding energy and R (~1.78 nm) denotes the exciton Bohr radius in trilayers[31]. Given the short lifetime of X_A (~picoseconds)[32,33] and thus the small density (~10^9 cm^{-2}, see Methods), the amount of blueshift is expected to be orders of magnitude smaller than the experimental values (and comparable to monolayers and bilayers[20,31]). On the other hand, although X_A can acquire a dipole moment via its hybridization with IX_D and experience X_A-X_I dipolar interaction with X_I, such interactions should have persisted in the intrinsic and electron-doped regime. Furthermore, we estimate an upper limit of dipolar interaction strength g_d ~ 1.8μeVμm^2, orders of magnitude smaller than the experimental interaction strength g (see Methods). This conclusion is supported by the experimental observation of much weaker nonlinearity of X_I than X_A^+, even when X_I is fully polarized by an external electric field (see Methods and **Fig. S10** for additional discussion).

Therefore, we attribute the observed nonlinearity to a valley polarization created from the interactions between X_A and free carriers. In particular, excitons created by optical pumping may

induce a nonequilibrium valley population imbalance of resident carriers between K and Γ valleys, via mechanisms such as exciton-carriers scattering[34,35]. Importantly, under zero electric field, the energy difference between K and Γ valleys is rather small in trilayers[22], on the order of tens of millielectronvolts, based on first-principle calculations and transport studies (**Fig. 3c**). As a result, electrostatically doped holes at the Γ point could be efficiently scattered into the K valley by excitons such as X_A and X_I, via Coulombic and exchange interactions[34,35] (**Fig. 3d**). This net accumulation of valley population at K (and K') induces phase space filling and, consequently, the observed blueshift of X_A^+. Such a scattering process would also introduce additional dephasing, which explains the increase in the X_A^+ linewidth. Meanwhile, the oscillator strength remains unchanged at low excitation power, since it depends on the total doping level, but decreases at higher power due to saturation. In addition to the exciton-carrier scattering, the net valley polarization may also be created by the electric field induced by optical pumping. For instance, it has been suggested in bilayer TMDs that the generation of dipolar X_I excitons may create a non-zero displacement field due to spontaneous symmetry breaking[1]. Such a displacement field can introduce a relative energy shift between K and Γ valleys[22], thus creating a valley polarization. To further investigate such possible valley polarization, we probe the population of the resident carriers in the K and K' valleys under circularly polarized resonant excitation. As shown in **Fig. S11**, we observe a stronger blueshift of X_A^+ in the K than K' valley when exciting excitons in the K valley, consistent with our optically induced valley polarization picture.

The proposed valley polarization mechanism also explains the strong electron-hole asymmetry of optical nonlinearity. Intrinsic trilayer WSe_2 exhibit weak nonlinearity, since no valley polarization can be created without resident carriers. In the electron-doped case, the valley polarization of

resident carriers is prevented by the much larger energy splitting, on the order of hundreds of millielectronvolts, between Q (band minimum) and the K valleys (where X_A resides) in the conduction band[22]. We also briefly note that in TMD monolayers, optical pumping with circularly polarized light can polarize carriers in K vs. K' valleys[32–38]. The generation of valley imbalance in monolayers has been attributed to mechanisms, such as different inter-valley vs. intra-valley carrier relaxation rates, and different indirect excitons and spin-forbidden dark excitons relaxation rates[39,40]. Unlike in monolayer, where a spin flip of carriers is required for scattering between K and K' valleys, the Γ point is spin-degenerate so that the intervalley scattering between K and Γ in trilayers can happen via a spin-conserving process, such as direct Coulomb and exchange interactions between holes and excitons. We note that X_I likely plays a crucial role in exciton-electron scattering owing to their larger population than X_A (see **Fig. S10** for estimated X_I density). Since relaxation processes of X_A to X_I and X_I to the ground state both involve finite momentum transfer, they can facilitate the valley polarization process via exciton-carrier scattering. This suggests that the dynamics of valley polarization could occur at a timescale similar to the X_I lifetime, on the order of nanoseconds, which may explain our observation of weaker nonlinearity created by the pulsed laser than CW with the same peak power (**Fig. S8**).

To further corroborate our hypothesis, we control the relative energies of Γ and K valleys by applying an external electric field[20,22], and study the resulting changes in both the energies and optical nonlinearity of Fermi polarons. First, we measure the reflectance of the X_A^+ and X_A^- as we change the electric field under fixed doping levels (**Fig. 4a & b**). With an increasing field, the energy of the X_A^+ blueshift at a smaller electric field and then switches to redshift above an electric field of ~0.05 V/nm (**Fig. 4a**). The electric field shifts the valence band maximum from Γ to K due

to the distinct orbit characters of the eigenstates[22]. While the eigenstate at K becomes layer-polarized with higher energies with the field, the wavefunction at Γ point features large interlayer coupling with small energy change under the field[22]. This shift from Γ to K leads to more phase space-filling in K and a blueshift of X_A^+, consistent with our proposed mechanism for optical nonlinearity (**Fig. S13**). Above an electric field of ~0.05 V/nm, X_A^+ begins to redshift. This electric field is comparable to the critical field under which band edge shifts from Γ to K, as determined from transport studies[22] (note the literature reported field differs from our definition by a factor of the relative dielectric constant). In stark contrast, the energy shift of the X_A^- is much smaller in electron-doped region (**Fig. 4b**), where the band edge remains at the Q point. The small energy variation of X_A^- can be explained by the avoided crossing similar to the undoped case (**Fig. S1**).

Intriguingly, the electric field also dramatically changes the nonlinear responses of X_A^+ . As shown in **Fig. 4c**, the reflectance change induced by optical pumping, $\Delta R/R$ shows a clear flip in the color contract at ~0.05 V/nm, which coincides with the crossover field between the blueshift and redshift of X_A^+ in **Fig. 4a.** The magnitude of blueshift and redshift is similar under the same excitation condition, around 10 meV (**Fig. 4d).** Such electric-field control of optical nonlinearity provides additional supporting evidence for our proposed mechanism involving valley polarization (**Fig. 4e, f**). **Figure 4e** shows the modified band structure above the critical field[22]. Under optical excitation, the same exciton-hole scattering process can induce a population transfer of holes from K to Γ, and reduce the X_A^+ energies (**Fig. 4f**). This also explains the similar critical electric fields where both nonlinearity and electric-field susceptibility turn from blue- to redshift.

Conclusion

Our results demonstrating highly nonlinear excitons with large oscillator strengths open avenues for engineering exciton-carrier interactions in atomically thin heterostructures to explore strongly interacting many-body physics and develop novel optoelectronics. By designing the atomic and electronic structures of the heterostructures, one may engineer the strong interactions between bright, dark excitons, and free charges[26]. The excitonic and free charge populations are highly tunable, and elucidating the complex interactions between intralayer, interlayer excitons, and charges will be of significant future interest for studying many-body physics in a hybrid Fermi-Bose system[41–43], from both theoretical and experiment perspectives. These strongly interacting optical excitations can be used to realize active nonlinear metasurfaces based on spatial confinement of excitons by moiré superlattice and local electrostatic gate[44–46]. Combining strong nonlinearity with spatial confinement could also further boost nonlinearity and allow exploring quantum optical effects, including nonclassical light sources and few-photon nonlinearity[11,47]. While current experiments require 10^3-10^4 photons to shift the resonance by a linewidth, improving materials quality and engineering photonic environment could lower required photon count significantly by reducing the Fermi polaron linewidth. Finally, the demonstrated optical control of exciton resonances could enable novel nonlinear optoelectronic devices such as all-optical switching, nonlinear optomechanical resonators[48,49], and optical limiting devices[4,50].

Acknowledgements:

This research is primarily supported by the U.S. Department of Energy, Office of Science, Office of Basic Energy Sciences Early Career Research Program under Award No. DE-SC-0022885. The fabrication of samples is supported by the National Science Foundation CAREER Award under Award No. DMR-2145712. This research used Quantum Material Press (QPress) of the Center for

Functional Nanomaterials (CFN), which is a U.S. Department of Energy Office of Science User Facility, at Brookhaven National Laboratory under Contract No. DE-SC0012704. K.W. and T.T. acknowledge support from the JSPS KAKENHI (Grant Numbers 20H00354, 21H05233 and 23H02052) and World Premier International Research Center Initiative (WPI), MEXT, Japan for hBN synthesis.

Author contributions

Y.Z. and L.G. conceived the project. L.G. fabricated the samples and performed the experiments. L.Z., R.N., S.P., and H.J. assisted with sample fabrication. L.Z. and R.N. helped with optical measurements. M.X., D.S.W. M.H. and Y.Z. contributed to the data analysis and theoretical understanding. T.T. and K.W. provided hexagonal boron nitride samples. L.G. and Y.Z. wrote the manuscript with extensive input from the other authors.

Competing financial interest

The authors declare no competing financial interests.

Additional Information

Supplementary information is available in the online version of the paper. Reprints and permission information is available online at www.nature.com/reprints. Correspondence and requests for materials should be addressed to youzhou@umd.edu.

References:

1. Datta, B. *et al.* Highly nonlinear dipolar exciton-polaritons in bilayer MoS2. *Nat. Commun.* **13**, 1–7 (2022).
2. Delteil, A. *et al.* Towards polariton blockade of confined exciton–polaritons. *Nat. Mater.* **18**, 219–222 (2019).
3. Muñoz-Matutano, G. *et al.* Emergence of quantum correlations from interacting fibre-cavity polaritons. *Nat. Mater.* **18**, 213–218 (2019).
4. Volz, T. *et al.* Ultrafast all-optical switching by single photons. *Nat. Photonics* **6**, 605–609 (2012).
5. Boyd, R. W. & Masters, B. R. Nonlinear Optics, Third Edition. *J. Biomed. Opt.* **14**, 029902 (2009).
6. Zasedatelev, A. V. *et al.* Single-photon nonlinearity at room temperature. *Nature* **597**, 493–497 (2021).
7. Chang, D. E., Sørensen, A. S., Demler, E. A. & Lukin, M. D. A single-photon transistor using nanoscale surface plasmons. *Nat. Phys.* **3**, 807–812 (2007).
8. Sun, S., Kim, H., Luo, Z., Solomon, G. S. & Waks, E. A single-photon switch and transistor enabled by a solid-state quantum memory. *Science* **361**, 57–60 (2018).
9. Mak, K. F. & Shan, J. Opportunities and challenges of interlayer exciton control and manipulation. *Nat. Nanotechnol.* **13**, 974–976 (2018).
10. Wilson, N. P., Yao, W., Shan, J. & Xu, X. Excitons and emergent quantum phenomena in stacked 2D semiconductors. *Nature* **599**, 383–392 (2021).
11. Wild, D. S., Shahmoon, E., Yelin, S. F. & Lukin, M. D. Quantum Nonlinear Optics in Atomically Thin Materials. *Phys. Rev. Lett.* **121**, 123606 (2018).

12. Liu, X. *et al.* Strong light–matter coupling in two-dimensional atomic crystals. *Nat. Photonics* **9**, 30–34 (2015).

13. Barachati, F. *et al.* Interacting polariton fluids in a monolayer of tungsten disulfide. *Nat. Nanotechnol.* **13**, 906–909 (2018).

14. Regan, E. C. *et al.* Emerging exciton physics in transition metal dichalcogenide heterobilayers. *Nat. Rev. Mater.* **7**, 778–795 (2022).

15. Zhang, L. *et al.* Highly valley-polarized singlet and triplet interlayer excitons in van der Waals heterostructure. *Phys. Rev. B* **100**, 041402 (2019).

16. Rivera, P. *et al.* Valley-polarized exciton dynamics in a 2D semiconductor heterostructure. *Science* **351**, 688–691 (2016).

17. Walther, V., Johne, R. & Pohl, T. Giant optical nonlinearities from Rydberg excitons in semiconductor microcavities. *Nat. Commun.* **9**, 1309 (2018).

18. Leisgang, N. *et al.* Giant Stark splitting of an exciton in bilayer MoS2. *Nat. Nanotechnol.* **15**, 901–907 (2020).

19. Louca, C. *et al.* Interspecies exciton interactions lead to enhanced nonlinearity of dipolar excitons and polaritons in MoS2 homobilayers. *Nat. Commun.* **14**, 3818 (2023).

20. Wang, Z., Chiu, Y. H., Honz, K., Mak, K. F. & Shan, J. Electrical Tuning of Interlayer Exciton Gases in WSe2 Bilayers. *Nano Lett.* **18**, 137–143 (2018).

21. Scuri, G. *et al.* Electrically Tunable Valley Dynamics in Twisted WSe2/WSe2 Bilayers. *Phys. Rev. Lett.* **124**, 1–8 (2020).

22. Movva, H. C. P. *et al.* Tunable Γ-K Valley Populations in Hole-Doped Trilayer WSe2. *Phys. Rev. Lett.* **120**, 107703 (2018).

23. Sidler, M. *et al.* Fermi polaron-polaritons in charge-tunable atomically thin semiconductors. *Nat. Phys.* **13**, 255–261 (2017).

24. Mak, K. F. *et al.* Tightly bound trions in monolayer MoS2. *Nat. Mater.* **12**, 207–211 (2013).

25. Wang, Z., Zhao, L., Mak, K. F. & Shan, J. Probing the Spin-Polarized Electronic Band Structure in Monolayer Transition Metal Dichalcogenides by Optical Spectroscopy. *Nano Lett.* **17**, 740–746 (2017).

26. Erkensten, D., Brem, S. & Malic, E. Exciton-exciton interaction in transition metal dichalcogenide monolayers and van der Waals heterostructures. *Phys. Rev. B* **103**, 045426 (2021).

27. Jones, A. M. *et al.* Spin-layer locking effects in optical orientation of exciton spin in bilayer WSe 2. *Nat. Phys.* **10**, 130–134 (2014).

28. Gong, Z. *et al.* Magnetoelectric effects and valley-controlled spin quantum gates in transition metal dichalcogenide bilayers. *Nat. Commun.* **4**, 2053 (2013).

29. Zhang, Y. *et al.* Every-other-layer dipolar excitons in a spin-valley locked superlattice. *Nat. Nanotechnol.* **18**, 501–506 (2023).

30. Stepanov, P. *et al.* Exciton-Exciton Interaction beyond the Hydrogenic Picture in a MoSe 2 Monolayer in the Strong Light-Matter Coupling Regime. *Phys. Rev. Lett.* **126**, 167401 (2021).

31. Scuri, G. *et al.* Large Excitonic Reflectivity of Monolayer MoSe2 Encapsulated in Hexagonal Boron Nitride. *Phys. Rev. Lett.* **120**, 37402 (2018).

32. Wang, G. *et al.* Valley dynamics probed through charged and neutral exciton emission in monolayer WSe 2. *Phys. Rev. B* **90**, 075413 (2014).

33. Hsu, W.-T. *et al.* Optically initialized robust valley-polarized holes in monolayer WSe2. *Nat. Commun.* **6**, 8963 (2015).

34. Courtade, E. *et al.* Charged excitons in monolayer WSe 2 : Experiment and theory. *Phys. Rev. B* **96**, 085302 (2017).

35. Fey, C., Schmelcher, P., Imamoglu, A. & Schmidt, R. Theory of exciton-electron scattering in atomically thin semiconductors. *Phys. Rev. B* **101**, 195417 (2020).

36. Yan, T., Yang, S., Li, D. & Cui, X. Long valley relaxation time of free carriers in monolayer WSe 2. *Phys. Rev. B* **95**, 241406 (2017).

37. Goryca, M., Wilson, N. P., Dey, P., Xu, X. & Crooker, S. A. Detection of thermodynamic "valley noise" in monolayer semiconductors: Access to intrinsic valley relaxation time scales. *Sci. Adv.* **5**, eaau4899 (2019).

38. Yang, L. *et al.* Long-lived nanosecond spin relaxation and spin coherence of electrons in monolayer MoS2 and WS2. *Nat. Phys.* **11**, 830–834 (2015).

39. Dery, H. & Song, Y. Polarization analysis of excitons in monolayer and bilayer transition-metal dichalcogenides. *Phys. Rev. B* **92**, 125431 (2015).

40. Robert, C. *et al.* Spin/valley pumping of resident electrons in WSe2 and WS2 monolayers. *Nat. Commun.* **12**, 5455 (2021).

41. Park, H. *et al.* Dipole ladders with large Hubbard interaction in a moiré exciton lattice. *Nat. Phys.* **19**, 1286–1292 (2023).

42. Gao, B. *et al.* Excitonic Mott insulator in a Bose-Fermi-Hubbard system of moiré WS2/WSe2 heterobilayer. Preprint at http://arxiv.org/abs/2304.09731 (2023).

43. Xiong, R. *et al.* Correlated insulator of excitons in WSe_2 /WS_2 moiré superlattices. *Science* **380**, 860–864 (2023).

44. Koshelev, K. *et al.* Subwavelength dielectric resonators for nonlinear nanophotonics. *Science* **367**, 288–292 (2020).

45. Bekenstein, R. *et al.* Quantum metasurfaces with atom arrays. *Nat. Phys.* **16**, 676–681 (2020).

46. Cai, T. *et al.* Radiative Enhancement of Single Quantum Emitters in WSe $_2$ Monolayers Using Site-Controlled Metallic Nanopillars. *ACS Photonics* **5**, 3466–3471 (2018).

47. Yu, H., Liu, G. B., Tang, J., Xu, X. & Yao, W. Moiré excitons: From programmable quantum emitter arrays to spin-orbit–coupled artificial lattices. *Sci. Adv.* **3**, 1–8 (2017).

48. Zhou, Y. *et al.* Controlling Excitons in an Atomically Thin Membrane with a Mirror. *Phys. Rev. Lett.* **124**, 27401 (2020).

49. Aspelmeyer, M., Kippenberg, T. J. & Marquardt, F. Cavity optomechanics. *Rev Mod Phys* **86**, 1391–1452 (2014).

50. Van Stryland, E. W., Wu, Y. Y., Hagan, D. J., Soileau, M. J. & Mansour, K. Optical limiting with semiconductors. *J. Opt. Soc. Am. B* **5**, 1980 (1988).

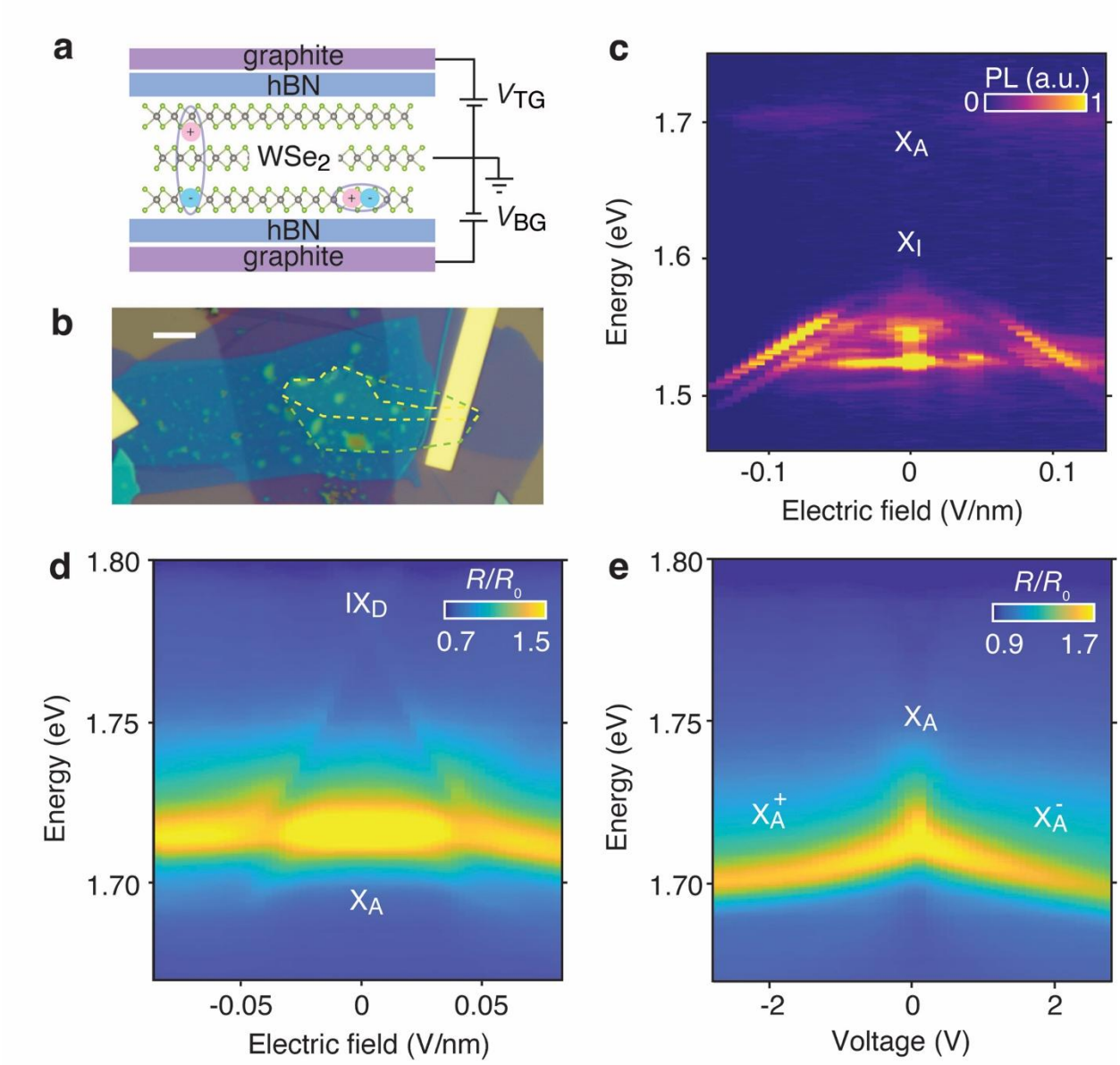

Figure 1. Dual-gated WSe_2 homotrilayer van der Waals heterostructure and their optical characteristics under gating at $T = 4$ K. a, a schematic of the trilayer vdWs heterostructure. The homotrilayer WSe_2 is encapsulated with two hBN of 15~20 nm thick. **b,** an optical image of the homotrilayer WSe_2 device (Scale bar: 5 μm). The trilayer and neighboring bilayer regions are enclosed by the yellow and green dashed line, respectively. **c,** Photoluminescence spectra of the WSe_2 trilayer under an electric field. The bright emission exhibiting a Stark shift under an electric field at 1.5 to 1.58 eV corresponds to the indirect exciton X_I. The upper weaker emission at 1.7 eV

corresponds to the momentum direct K-K intralayer exciton X_A. **d,** Reflectance spectra of the WSe_2 trilayer under an electric field. The high energy momentum direct K-K interlayer exciton shows a Stark shift of ~100 meV and begins to hybridize with X_A when their energies become degenerate around the electric field of 0.05 V/nm. **e,** Doping-dependent reflectance spectra of the WSe_2 trilayer. With increasing doping concentration, the intralayer trion or Fermi polaron (X_A^-/X_A^+) shifts toward lower energy.

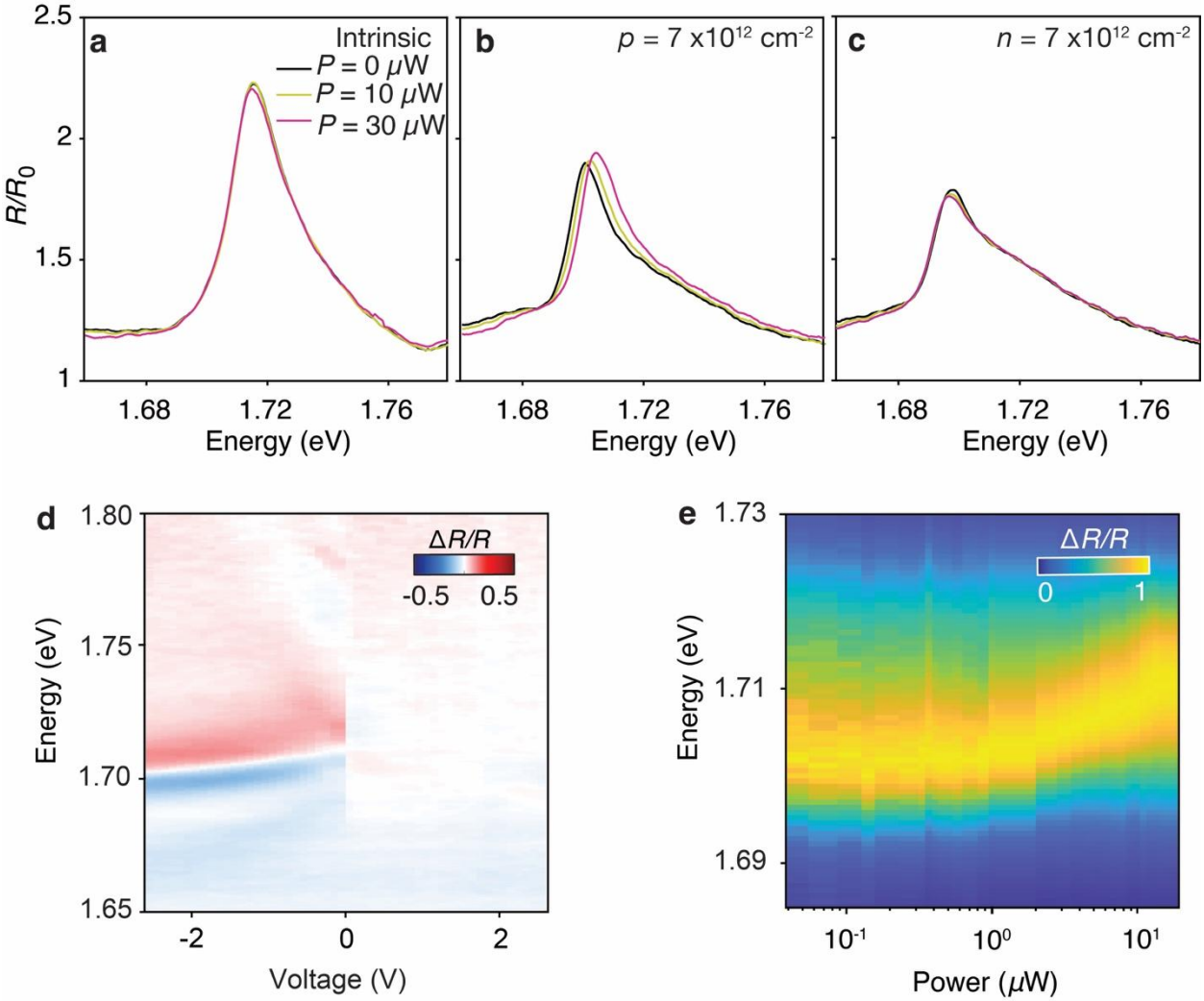

Figure 2. Nonlinearity in hole-doped homotrilayer WSe_2 at $T = 4$ K . a, b, c, Reflectance contrast R/R_0 of the trilayer under 0 μW, 10 μW, 30 μW CW (635nm) laser excitation with different doping levels, where R_0 is the reflectance of a reference region near the trilayer region with bare graphite/hBN/graphite on SiO_2 on the sample. Intriguingly the exciton blueshifts when the sample is hole-doped. **d,** Relative change in the reflectance induced by 30 μW of CW laser pumping under different doping. The color map is obtained by normalizing the reflectance change induced by the CW excitation with respect to the reflectance without optical pumping, $\Delta R/R = \frac{R_{(30\mu W)}}{R_{(No\ Pump)}} - 1$. Therefore, a positive value (red color) at high energy and negative

value (blue) at low energy indicates a blueshift. The apparent discontinuity near 0V is due to the high excitation power and finite voltage step used, and such transition becomes smoother at lower excitation power (see **Fig. S7** for additional data). **e,** Blueshift of the X_A^+ as a function of the pulsed laser excitation (718-720nm, resonant with X_A^+) power, with a hole doping level of $7 \times 10^{12} cm^{-2}$. The seeming redshift in the peak energy below 1 μW is due to fluctuations. In fact, X_A^+ consistently shifts toward higher energy with increasing power (see **Fig. S8** for additional data and analysis).

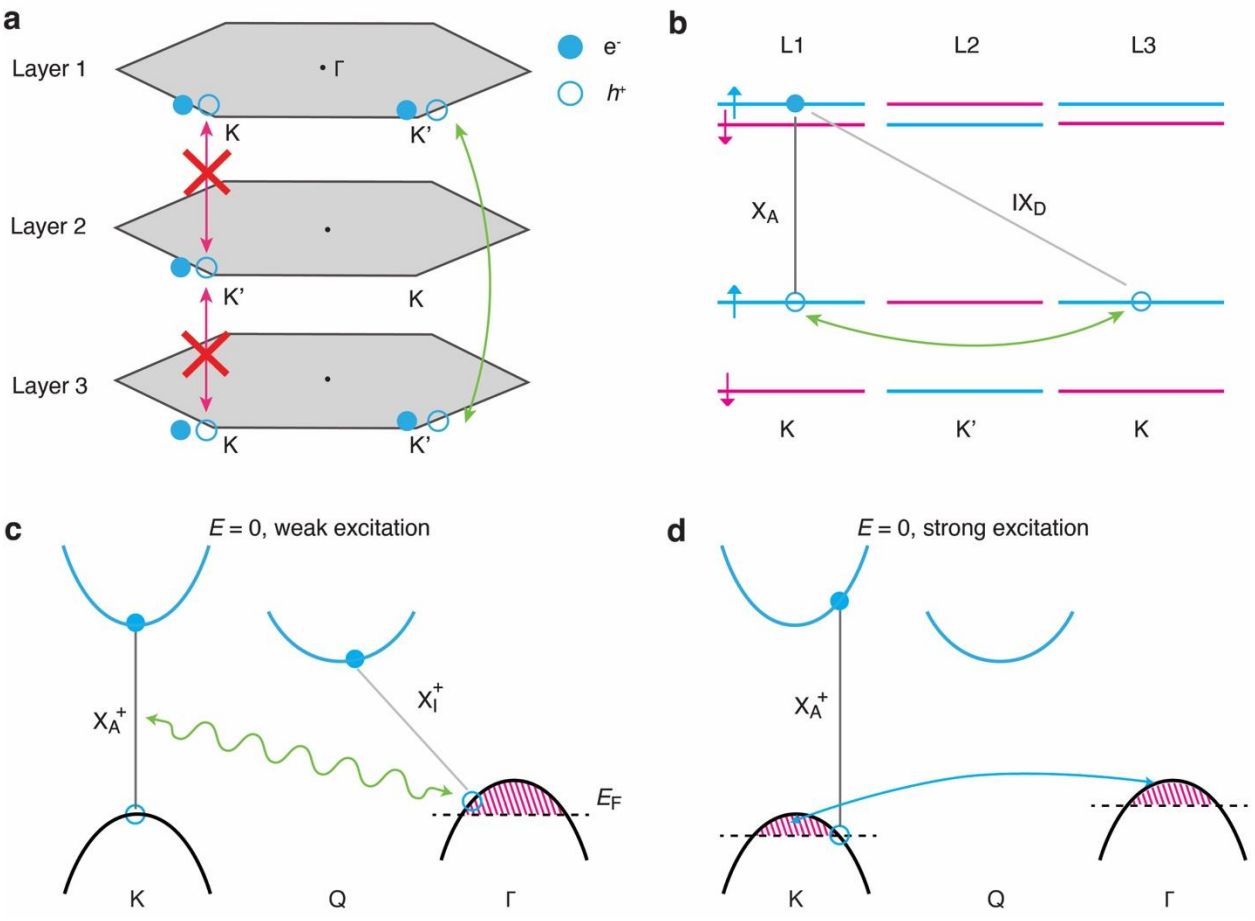

Figure 3. Electronic band structure of trilayer WSe_2. a, The crystal structure of natural trilayer WSe_2 dictates alternating K and K' valleys among neighboring layers. The strong spin-orbit coupling of holes leads to weak tunneling among neighboring layers but strong tunnelling between the top and bottom layer. **b,** The tunnelling of holes between top and bottom layer results in the hybridization of intralayer K-K excitons X_A and interlayer K-K excitons IX_D. **c, d,** Band structures and carrier populations of hole-doped trilayer WSe_2 in the absence of electric field(E = 0). **c,** Optical excitation generates both momentum direct intralayer X_A^+ and momentum indirect X_I of higher population. Intralayer Fermi polaron X_A^+ can interact with X_I and the free holes in the system. **d,** Under strong optical excitation, the interaction between intralayer

excitons and free charges can induce a population transfer of carriers from the Γ to the K valley. The energy difference between Γ and K is small. The additional free carriers in K valley leads to phase space filling and optically induced blueshift of X_A^+. We note that in this nonequilibrium state, the dashed lines do not represent the Fermi level but are indications for the carrier population.

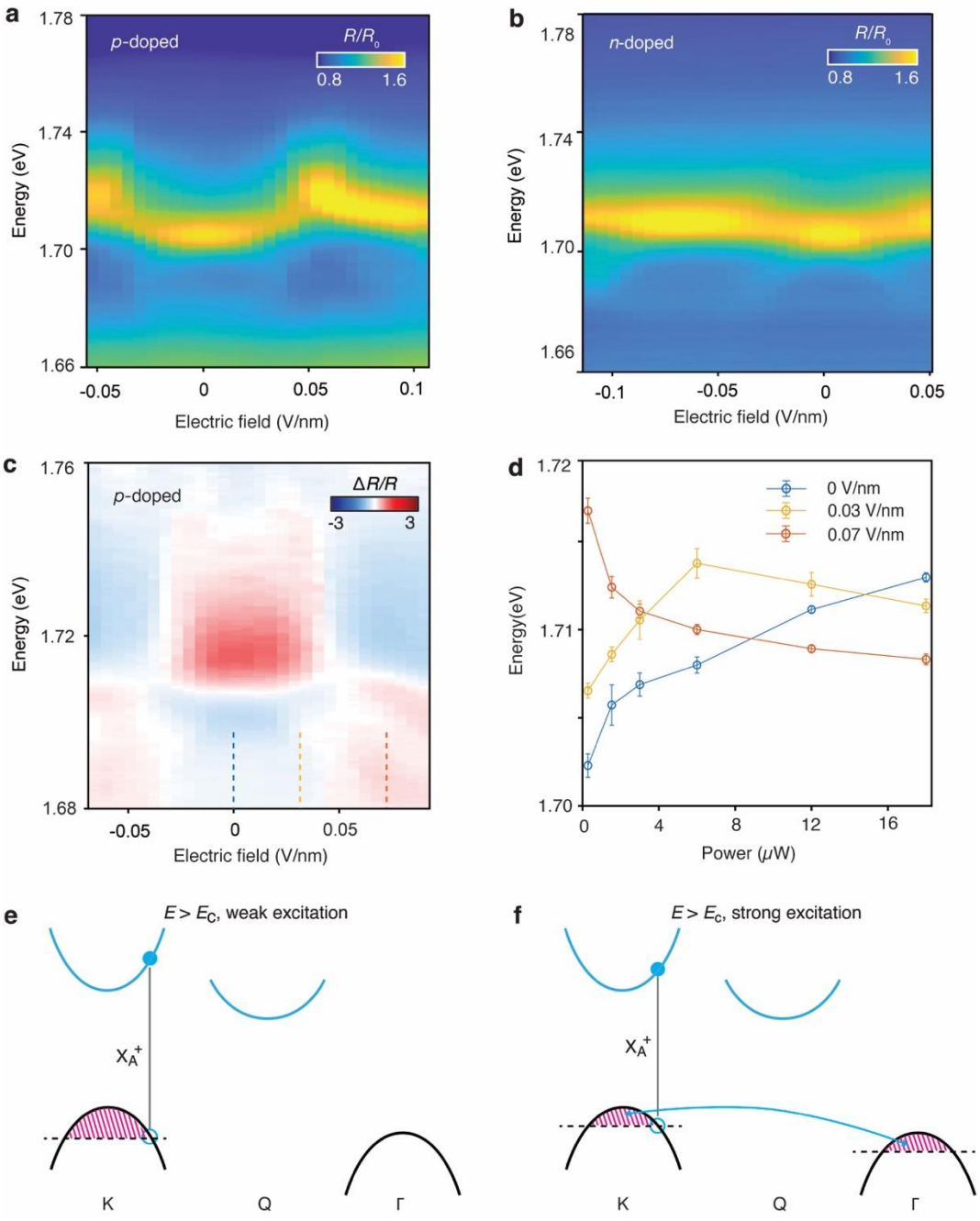

Figure 4. Electric-field dependent exciton energy and nonlinearity in homotrilayer WSe_2 at $T = 4$ K. a, b, Electric field dependence of the intralayer Fermi polaron reflectance contrast R/R_0 in trilayer with a (**a**) hole and (**b**) electron doping density of $4.9\times 10^{12} cm^{-2}$. **c,** Reflectance change induced by a pulsed laser excitation of 12 μW power. The color map is obtained the same way as Fig. 2d. Under a small electric field, X_A^+ shows a blueshift but it begins to redshift under

excitation at higher electric field. **d,** Line plots of the X_A^+ power-dependent peak shift under different electric fields. The X_A^+ shows a blue shift of ~10 meV under zero applied electric field and a redshift of similar magnitude under large electric field. The corresponding electric fields for these linecuts are indicated by the dashed lines in (**c**). **e, f,** An electric field induces a shift of the valence band edge from Γ to K valley. Under strong optical pumping, a net valley polarization is induced by exciton-carrier scattering with increased carriers at the Γ point, which leads to the optically induced redshift of X_A^+ at higher electric field. In the nonequilibrium states, the dashed lines are used as indications for the carrier populations, and do not represent the Fermi level.

Methods:

Device fabrication

Graphite, hBN flakes are mechanically exfoliated from the bulk crystals onto the silicon chip with SiO_2 layer. Some of the exfoliated homotrilayer WSe_2 flakes were provided by the Quantum material press (QPress) facility in Center for functional nanomaterials (CFN) at Brookhaven national laboratory (BNL). The thickness of the hBN flakes and WSe_2 layer numbers are estimated based on the colour contrast under the optical microscopy. The heterostructure is assembled in a transfer station built by Everbeing Int'l Corp., which use PDMS(Polydimethylsiloxane) and PC (Polycarbonate) as stamp and transfer all the flakes in a dry transfer method onto a silicon chip with 285nm SiO_2 layer. Then the electrical contacts are patterned by electron-beam lithography and a liftoff process where we deposited 5nm of Cr and 80nm of Au by thermal evaporation.

Optical spectroscopy

The optical measurements were performed in our home-built confocal microscope with Attodry 4K cryostat. The apochromatic objective equipped in the chamber has numerical aperture NA=0.82. The PL measurement is performed with a 635nm diode laser excitation. The reflectance measurement is performed using either a halogen lamp (from Thorlabs) or a supercontinuum white laser (from YSL Photonics Inc.) as the excitation source. The diode laser has a diffraction-limited spot size while the beam diameter of the white laser is slightly larger, around $1\mu m$. The white laser has a pulse duration of ~60 ps with variable repetition rate up to 40 MHz. Our power-dependent reflectance is measured under both continuous wave and pulsed excitation. In CW measurements, we illuminate the sample with the halogen lamp as the probe and use the CW (635nm) diode laser as excitation with a power ranging from 0.02 to 30 microwatts. In the pulsed resonant excitation

case, we excite the system with a supercontinuum white laser filtered to 718-730nm wavelength range. We vary the incident power and directly measure the reflected white laser signal from the sample. In both cases, our reflectance spectral is normalized by dividing the reflected light intensity from the sample trilayer area by the reflected light intensity from the nearby bare hBN on SiO_2 area. The spectra is measured by a Horiba iHR320 spectrometer using a 300mm/line grating and a Synapse-Plus back-illuminated deep depletion CCD camera.

Doping Density and Electric field

The doping density and electric field are determined by considering the heterostructure as a parallel capacitor[30]. The applied electric field is calculated as $E = \frac{D}{\varepsilon_0 \varepsilon_{WSe2}}$, while the D displacement field is determined by $D = \frac{1}{2}(C_{Top} \cdot \Delta V_{TG} - C_{Bottom} \cdot \Delta V_{BG})$. The top and bottom capacitance are given by $C_{Top(Bottom)} = \frac{\varepsilon_0 \varepsilon_{hBN}}{t_{hBN}}$, where *t* is the thickness of top and bottom hBN. ΔV_T and ΔV_B is the applied top and bottom gate voltage relative to the offset voltage to the band edge, respectively. The total doping density in the system can be determined as $n = \frac{1}{e} \cdot (C_{Top} \cdot \Delta V_{TG} + C_{Bottom} \cdot \Delta V_{BG})$. We use $\varepsilon_{WSe2} = 7$, [33,41] $\varepsilon_{hBN} = 3$, [41] in our case. The thicknesses of hBN layers are extracted by atomic force microscope measurements.

Extract Dipole Distance *d*

The energy shift as a function of the electric field of the IX_D and X_I obeys the law of the stark shift, which can be described as:

$$\Delta E = |e \cdot d \cdot E| = |e \cdot d \cdot \frac{\varepsilon_{hBN}}{\varepsilon_{WSe2}} \cdot \frac{V_{BG}}{t_{BG}}| \quad (1)$$

Thus the dipole moment of excitons can be calculated as

$$d = |\frac{\Delta E}{e} \cdot \frac{\varepsilon_{WSe2}}{\varepsilon_{hBN}} \cdot \frac{t_{BG}}{V_{BG}}| \quad (2)$$

Estimate of exciton density

In the steady state, the exciton densities of both intra- and inter-layer excitons can be estimated by $n_X = I\alpha\tau/A\hbar\omega$, where I is the pump power, A is the pump beam size, $\hbar\omega$ is the photon energy, α is the sample's absorbance at the pump wavelength, and τ is the lifetime of respective excitons. The lifetime of interlayer excitons X_I is estimated from time-dependent PL measurements, while we take the lifetime of X_A from literature.

The density of X_I can be estimated from an independent method by measuring their PL and considering dipolar interactions using a simple capacitor model in which the exciton density is proportional to the blue shift induced by the repulsion between excitons[20]: $n_x = \frac{\varepsilon_0 \varepsilon_{tmd} \cdot \Delta E}{de^2}$, where ΔE is the blueshift of the emission energy and d is the dipole moment of X_I, estimated to be ~0.78nm from the Stark effect.

Estimate of exchange and dipolar interaction strength

The exchange interaction strength can be estimated from $g_{ex} \sim \alpha E_B R^2$, where α is a constant, E_B is the exciton binding energy and R denotes the exciton Bohr radius in trilayers. For our calculation, we adopt $\alpha = 6$, E_B of ~100 meV, R of 1.78 nm, which are values from literature[31], to estimate the interaction strength.

Meanwhile, X_A could acquire finite electrical dipoles via its hybridization with IX_D. We note that to the first order, there should be zero net dipoles and weak dipolar interactions under symmetric gating. However, the emergence of local net dipoles is plausible due to spontaneous symmetry

breaking. In light of this, we calculate an upper limit for the dipolar interactions, assuming all dipoles are aligned. Using a parallel plate model, the dipolar interaction strength is given by $g_d = \frac{e^2 d}{\varepsilon_0 \varepsilon_{TMD}}$, where ed is the dipole moment of X_A. This dipole moment, ed, acquired from the hybridization with IX_D, can be estimated from the composition percentage of each exciton species in the coupled oscillator model (Fig. S2). The value peaks when X_A become degenerate with IX_D reaching ~0.7 $nm \cdot e$, and leading to an estimated dipolar interaction strength of g_d ~1.7 μeVμm^2.

Estimate of photon numbers required to shift the resonance by a linewidth

The photon numbers are calculated from $n = \frac{P\tau}{E}$ where P is the power of the laser, τ is the Fermi polaron lifetime, and $E = \frac{hc}{\lambda}$ is the photon energy. For pulsed laser excitation, we convert the average pumping power (P_{Avg}) into peak power $P = \frac{P_{Avg}}{f_R \cdot t_p}$, with f_R is repetition rate and t_p is the pulse duration.

Data availability

Source data are provided with this paper. All other data are available from the corresponding authors upon reasonable request.